Atmos. Chem. Phys., 14, 6925–6940, 2014
www.atmos-chem-phys.net/14/6925/2014/
doi:10.5194/acp-14-6925-2014
© Author(s) 2014. CC Attribution 3.0 License.

Atmospheric Chemistry and Physics
Open Access

Factors controlling pollutant plume length downwind of major roadways in nocturnal surface inversions

W. Choi[1], **A. M. Winer**[2], **and S. E. Paulson**[1]

[1]University of California, Los Angeles, Department of Atmospheric and Oceanic Sciences, Los Angeles, California, USA
[2]University of California, Los Angeles, School of Public Health, Environmental Health Sciences Department, Los Angeles, California, USA

Correspondence to: S. E. Paulson (paulson@atmos.ucla.edu)

Received: 19 April 2013 – Published in Atmos. Chem. Phys. Discuss.: 30 September 2013
Revised: 2 April 2014 – Accepted: 28 May 2014 – Published: 4 July 2014

Abstract. A fitting method using a semi-empirical Gaussian dispersion model solution was successfully applied to obtain both dispersion coefficients and a particle number emission factor (PNEF) directly from ultrafine particle (UFP; particles smaller than < 0.1 µm in diameter) concentration profiles observed downwind of major roadways in California's South Coast Air Basin (SoCAB). The effective Briggs' formulation for the vertical dispersion parameter σ_z was adopted in this study due to its better performance in describing the observed profiles compared to other formulations examined. The two dispersion coefficients in Briggs' formulation, α and β, ranged from 0.02 to 0.07 and from -0.5×10^{-3} to 2.8×10^{-3}, respectively, for the four freeway transects studied and are significantly different for freeways passing over vs. under the street on which measurements of the freeway plume were made. These ranges are wider than literature values for α and β under stable conditions. The dispersion coefficients derived from observations showed strong correlations with both surface meteorology (wind speed/direction, temperature, and air stability) and differences in concentrations between the background and plume peak. The relationships were applied to predict freeway plume transport using a multivariate regression, and produced excellent agreement with observed UFP concentration profiles. The mean PNEF for a mixed vehicle fleet on the four freeways was estimated as 7.5×10^{13} particles km^{-1} vehicle^{-1}, which is about 15 % of the value estimated in 2001 for the I-405 freeway, implying significant reductions in UFP emissions over the past decade in the SoCAB.

1 Introduction

Ultrafine particles (UFP) are generally defined as particles smaller than 0.1 µm in diameter (Morawska et al., 2008). Numerous epidemiological and toxicological studies have shown that UFP cause various adverse health effects, such as respiratory illness, DNA damage, cardiovascular disease, and adverse birth outcomes (Hoek et al., 2010; Knol et al., 2009; Moller et al., 2008). The dominant source of UFP in urban areas is vehicular emissions (Pey et al., 2009). UFP in urban areas account for the major proportion (∼ 80%) of total particulate matter (PM) number concentration but a negligible proportion of the mass concentration (Kumar et al., 2010). However PM mass ($PM_{2.5}$ and PM_{10}) is currently regulated but PM numbers are not, thus measurements of ambient UFP are relatively sparse.

Although a number of studies on UFP emissions from major roadways and their spatial impacts have recently been conducted, the meteorological conditions in most studies were limited to the daytime unstable convective boundary layer (Karner et al., 2010). However, Hu et al. (2009) found a wide UFP impact area up to 2 km downwind of the I-10 freeway during stable pre-sunrise hours in Santa Monica, California. Subsequently, Choi et al. (2012) extended this result, reporting the prevalence of wide area impacts (1500 m to more than 2500 m) downwind of freeways under stable pre-sunrise conditions at several additional locations throughout the South Coast Air Basin (SoCAB). Choi et al. (2012) also found the decay constant of UFP concentrations with distance under stable conditions is about an order of magnitude smaller than that during daytime.

While the dominant factor causing differences in dispersion/dilution rates between nocturnal (stable) and daytime (well mixed) conditions is clearly atmospheric stability combined with different boundary layer heights (Kerminen et al., 2007; Hu et al., 2009; Hussein et al., 2006; Zhu et al., 2006), quantitative and systematic meteorological dependencies of the decay of primary pollutants with distance downwind of major roads have yet to be developed, particularly for stable atmospheres. This gap prevents the reliable prediction of the extent and magnitude of roadway plumes under stable conditions when their greater downwind extent potentially impacts large populations.

Many studies have attempted to predict the pollutant concentrations from vehicular emissions near roadways using different dispersion models with varying levels of complexity (Sharma and Khare, 2001). However, most studies have focused on predicting elevated pollutant concentrations at specific distances from sources rather than describing concentration profiles. A few studies attempted to reproduce UFP concentration profiles obtained at multiple discrete distances within short ranges (< 300 m) during daytime conditions (Zhu and Hinds, 2005; Gramotnev et al., 2003; Heist et al., 2013).

Gaussian dispersion models have been commonly used to explain spatial concentration variations from line sources (e.g., Sharma and Khare, 2001; Chen et al., 2009; Briant et al., 2011; Gramotnev et al., 2003; Kumar et al., 2011; Heist et al., 2013). Simple Gaussian models require parameterization of dispersion coefficients, which is critical to calculate pollutant concentrations at specific distances from the source. Existing parameterizations of the dispersion coefficients for these models are based on Pasquill stability classes (Pasquill, 1961). However, the Pasquill parameterization has only two classes for stable conditions (Table 1), and thus has limited ability to explain the variations in concentration profiles under stable conditions. In addition, current sophisticated dispersion models (such as AERMOD, CALINE, RLINE, etc.) require a comprehensive data set including friction velocity, surface heat flux, boundary layer and mechanical mixing heights, surface roughness, vertical wind profiles, complex roadway configurations, etc. (Heist et al., 2013). Detailed turbulence measurements as well as boundary layer and mechanical mixing heights and surface roughness, etc. cannot be readily and routinely obtained in urban areas. In addition, these requirements prevent direct and quantitative comparison between input variables and observed concentration profile shapes, regardless of the model performance. Although many modeling studies estimate turbulence parameters based on the Monin–Obukhov similarity theory, the theory is not perfect for the real atmosphere and particularly under stable nocturnal conditions, which is typically the most challenging situation for current dispersion models (Heist et al., 2013). We also note that for our sampling periods (04:30 to 06:30 local time, LT), traffic flows on the target highways are sharply increasing due to the development of the morning commute, which is, we think, difficult to represent even with the current comprehensive models. While these more complex sophisticated models are ideal for many applications, here we probe how routinely measured variables (basic meteorological parameters and concentration data) affect UFP plume shapes, and thus have chosen to use a semi-empirical Gaussian expression for our investigation.

In the present study, the objectives are to investigate how routinely measured variables affect UFP plume magnitude, transport, and concentration decay rates, and consequently to evaluate the areal impact of traffic plumes from major roadways. For this reason, the effectiveness of the analytical solution for Gaussian dispersion to fit observed UFP concentration profiles is examined, and both dispersion coefficients and emission factors are obtained directly from the observations in this study. In addition, the quantitative effects of surface meteorological parameters and the role of concentration differences between plumes and backgrounds on plume extensions are investigated. Appropriate parameterization of dispersion coefficients and emission factors based on observable variables can provide predictive capability for the extent of freeway plumes under stable conditions.

2 Methods

2.1 Sampling areas and transects

The analyses are carried out for the detailed data set collected by Choi et al. (2012) with a mobile measurement platform (MMP) in the early morning before sunrise at four locations in the SoCAB. The downtown Los Angeles (DTLA), Paramount, Carson, and Claremont transects traveled along N. Coronado St., Obispo St., 228th St., and N. Mountain Ave., respectively, and crossed perpendicular to the respective freeways, the 101, 91, I-110, and I-210 freeways. The DTLA transect was located ∼ 22 km from the ocean, and the Paramount and Carson transects were located about 8–10 km from the ocean, whereas the Claremont transect was located further inland (∼ 50 km east from DTLA and ∼ 70 km from the coast), at the foot of the steeply rising San Gabriel Mountains (Supplement Fig. S1). All transects were small two-lane streets through residential areas surrounded mostly by one-story single family homes. For the DTLA and Paramount transects, the 101 and 91 freeways passed over the measurement routes, and for the Carson and Claremont transects, the I-110 and I-210 freeways passed under the routes as illustrated in Supplement Fig. S2. More details about transects and surroundings are provided in Choi et al. (2012) and in the Supplement Sect. S1.

2.2 Instrumentation, sampling, and data analysis

A pollution-free Toyota RAV4 sub-SUV electric vehicle served as the MMP in the present study. Vehicle production of UFP from brake wear and other related sources are

Table 1. Parameterizations of σ_z for Gaussian and K-theory dispersion models and σ_z values obtained from transect-averaged ultrafine particle concentration profiles in this study.

References	Equation form	Land use	Stability class	σ_z or γ[b] formula	
Chock (1978)	$\sigma_z = (a + b \cdot x)^c$	N/A	Stable	$a = 1.49$, $b = 0.15$, $c = 0.77$	
Briggs (1973)	$\sigma_z = \frac{\alpha \cdot x}{1+\beta \cdot x}$	Rural	E[a] (slightly stable)	$\alpha = 0.03$	
				$\beta = 0.3 \times 10^{-3}$	
			F[a] (moderately stable)	$\alpha = 0.016$	
				$\beta = 0.3 \times 10^{-3}$	
	$\sigma_z = \frac{\alpha \cdot x}{\sqrt{1+\beta \cdot x}}$	Urban	E − F[a] (stable)	$\alpha = 0.08$	
				$\beta = 1.5 \times 10^{-3}$	
Sharan and Yadav (1998)	$\gamma = (\sigma_w/\mathrm{U})^2$	N/A	Stable or unstable	$\sigma_w = \sqrt{\overline{(w - \overline{w})^2}}$	
This study (transect averaged σ_z	$\sigma_z = \frac{\alpha \cdot x}{1+\beta \cdot x}$	Urban to	Near neutral to stable	DTLA (R^2 =0.96)	$\alpha = 0.07$ $\beta = 0.4 \times 10^{-3}$
and R^2 for semi-empirical GB model)		suburban	pre-sunrise periods	Paramount	$\alpha = 0.034$
				(R^2 =0.96)	$\beta = -4.6 \times 10^{-4}$
				Carson	$\alpha = 0.02$
				(R^2 =0.91)	$\beta = 0.6 \times 10^{-3}$
				Claremont	$\alpha = 0.03$
				(R^2 =0.87)	$\beta = 2.8 \times 10^{-3}$

[a] D, E, and F are Pasquill stability classes for nighttime conditions (Pasquill, 1961). [b] γ represents a turbulence parameter used in Sharan and Yadav (1998), where σ_w is turbulence intensity in vertical direction, w is vertical wind component, and U is the mean wind speed.

expected to be small; see Supplement Sect. S2. UFP measurements were conducted with 1 s time resolution using a fast mobility particle sizer (FMPS) and condensation particle counter (CPC). Measurements of nitric oxide, carbon monoxide, particle-bound polycyclic aromatic hydrocarbons, $PM_{2.5}$, PM_{10}, and black carbon were also conducted. Instruments and calibrations are described in detail elsewhere (Choi et al., 2012; Hu et al., 2009; Kozawa et al., 2009; Westerdahl et al., 2005). Here we focus on UFP concentration profiles during the stable pre-sunrise hours in the SoCAB. UFP provide the clearest profiles, due to a combination of fast response instrumentation and a greater dynamic range of pollutant concentrations. The latter results from a low background level, due to the relatively short UFP lifetime (Capaldo and Pandis, 2001). We note that here we use UFP measured with a condensation particle counter (CPC), which counts particles in the 10 to 1000 nm range. These numbers are not differentiable from FMPS measurements for particles smaller than 100 nm, as particles smaller than 100 nm contributed 95.9 to 98.3 % of total FMPS numbers for all measurements.

Measurements were conducted during the pre-sunrise hours (04:30–06:30 LT) in the winter to spring seasons for the DTLA, Paramount, and Carson transects (January to March), and in Claremont during May and June of 2011 (Table 2). The MMP was driven at roughly constant slow speeds (below 30 km h^{-1}) during sampling whenever possible (allowing for stop signs and traffic lights). Data were logged every second. In order to synchronize the instrumental response times, a time-lag correlation method was used (Choi et al., 2012). Local impacts of individual high-emission vehicles encountered on a transect were removed by a running low 25 % quantile method (Choi et al., 2012). Any remaining local effects were examined and removed by reviewing video and audio records to verify proximity of a high-emitting vehicle. More details about instrumentation, sampling, and post-sampling data analyses are found in Supplement Sect. S2 and Choi et al. (2012).

Averaged surface meteorology (temperature, wind speed and direction, and relative humidity) was obtained with 2-D sonic anemometer and temperature/humidity sensors located on the roof the MMP, for about 5 min just prior to and following every transect run. Vertical gradients of temperature, humidity, and wind speed/direction were obtained once per day with a balloon tethersonde (SmartTether™, Anasphere Inc.) before the measurements at locations within 1 to 4 km of the transects. Closer proximity was not possible because of the high density of airports and airstrips (regulations prohibit tethered balloon flights within 8 km of an airport) and urban development, which provides few unobstructed areas for balloon-borne measurements. Traffic flow data were collected for the four freeways from the Freeway Performance Measurement System (PeMS) operated by the Institute of Transportation at University of California, Berkeley. The locations of traffic flow sensors and other details concerning general meteorological and traffic conditions during the sampling periods are available in Choi et al. (2012) and Supplement Sect. S3.

2.3 Theory and fits of observational data

2.3.1 Development of a semi-empirical formulation

An analytical Gaussian dispersion solution with the slender plume approximation assuming an infinite line source and the total reflection at the surface was applied as a basic expression, and fit to the observed concentration profiles

Table 2. Summary of measurements, estimated emission parameters, Q_c, and dispersion coefficients (α and β) from the semi-empirical GB model. All measurements were made within the period 04:30 to 06:30 a.m. LT and were completed before the local sunrise time.

Sampling area (transect street)	Date	Background conc.[a] ($\times 10^3$)	Q_c ($\times 10^4$)	α	β ($\times 10^{-3}$)	Temp.[b] (°C)	Model fit condition
Downtown LA	2/24/11	16.1	1.34	0.059	0.81	7.6	$H = 6$ m
(Coronado St.)	3/7/11	4.7	0.93	0.105	1.79	12.8	$z = 1.5$ m
	3/9/11	14.7	0.99	0.056	0.15	13.3	
	3/14/11	13.0	1.15	0.085	1.72	11.7	
	3/17/11	16.1	0.63	0.089	1.21	15.0	
Paramount	1/27/11	19.3	1.86	0.038	−0.19	9.8	$H = 6$ m
(Obispo St.)	2/1/11	18.3	1.83	0.045	−0.12	8.9	$z = 1.5$ m
	3/10/11	12.4	1.32	0.048	−0.34	12.2	
	3/15/11	6.1	1.70	0.063	0.58	12.2	
	3/18/11	19.8	1.94	0.038	−0.43	10.0	
West Carson	1/21/11	23.6	0.63	0.024	1.29	7.5	$H = 0$ m[c]
(228th St.)	2/3/11	21.6	0.74	0.016	0.09	2.8	$z = 1.5$ m
	3/8/11	11.0	0.43	0.034	1.51	12.1	
	3/11/11	14.2	0.56	0.020	−0.14	9.5	
	3/16/11	15.3	0.27	0.035	3.85	13.1	
	3/29/11	12.3	0.58	0.023	0.14	8.9	
Claremont	5/19/11	4.8	0.38	0.030	3.42	6.0	$H = 0$ m[c]
(Mountain Ave.)	5/24/11	6.4	0.26	0.035	5.37	8.9	$z = 1.5$ m
	5/25/11	7.2	0.32	0.066	7.29	9.5	
	5/26/11	7.0	0.39	0.020	1.44	8.9	
	6/1/11	5.1	0.31	0.050	5.18	7.4	
	6/2/11	7.4	0.50	0.029	2.27	7.1	
	6/7/11	7.1	0.26	0.048	4.55	9.6	

[a] Background concentrations are defined as a lower 25 % quantile point in the upwind area. [b] Mean temperature during pre-sunrise sampling period. Temperatures ranged within ±0.5 °C or less on each sampling day. [c] Actual height of the freeway surface is about 6 m below the transect. However, it is assumed that a freeway plume is well mixed within the freeway area due to mechanical turbulence produced by vehicle wakes and then rolls up to the measurement transect.

(Eq. 1):

$$C(x,z) = \frac{Q}{\sqrt{2\pi}\sigma_z(x)\cdot U_e}\left[\exp\left(-\frac{(z+H)^2}{2\sigma_z^2(x)}\right)+\exp\left(-\frac{(z-H)^2}{2\sigma_z^2(x)},\right)\right] \quad (1)$$

where Q is an emission rate, U_e is an effective wind speed (ambient wind + speed correction due to traffic wake), z is height, H is the height of the emission source, and σ_z is the standard deviation of the time-averaged concentration distributions in the vertical direction at distance x from the source (Luhar and Patil, 1989). An infinite line source assumption is reasonable for the present study due to the long length of freeways (more than 20 km) compared to relatively short downwind length scale of transects (~ 2 km). An assumption of total absorption at the surface may be more suitable for actual behavior of UFP. However, we note that the analytical solution with this assumption yields $C(x,z) = 0$ for the ground source ($H = 0$) (see Eq. 18.8 in Seinfeld and Pandis, 1998), which is the case for underpass freeway transects in the present study (Sect. 2.1 and Supplement Sect. S2). However, the most insights are likely to be gained from using the same assumptions and analytical form for the different freeway-transect geometries examined here. Although total reflection at the ground is not accurate, it would be reasonable to assume the reflectivity/absorption will not vary significantly at the paved urban surfaces, and hence the effect of the reflectivity assumption on σ_z should vary little among different sampling sites. The reflection at the top of boundary layer is not considered because a neutral/mixed residual layer exists over the nocturnal surface inversion. Consequently, this simple analytical Gaussian dispersion solution was chosen as a basic equation to minimize the number of free variables to fit to the observations, leading to results that are consistent and reliable and can be effectively interpreted.

Equation (1) may be simplified to obtain a final semi-empirical Gaussian expression (Eq. 2), in which Q_c represents a bulk emission parameter including emission rate (Q) combined with wind effects (U_e), and remains as a free variable to be determined from observed concentration profiles.

$$C(x,z) = \frac{Q_c}{\sigma_z}\left[\exp\left(-\frac{(z+H)^2}{2\sigma_z^2}\right)+\exp\left(-\frac{(z-H)^2}{2\sigma_z^2}\right)\right] \quad (2)$$

The final step to formulate a simplified model equation is to parameterize σ_z. For this, two common methods were examined: Chock (1978) and Briggs (1973) formulas. These were used by Luhar and Patil (1989) and Briant et al. (2011), respectively, in their model evaluations. However, we note that both Chock's and Briggs' formulas have just one or two equations for stable atmospheres, in each case based on land use (e.g., urban and rural). Thus, neither formula is sufficient to explain the meteorology-dependent variations in observed freeway plume decay during stable pre-sunrise hours. To account for these limits, two coefficients in Chock's and Briggs' formulas were held as free variables in the semi-empirical Gaussian equation (e.g., α and β for Briggs formula in Eq. 3). We found that the Briggs' formula form more successfully described the observed concentration profiles. Fitted results using Chock's formula tended to underestimate the peak concentrations near freeways. Additionally, we examined a K-theory model developed by Sharan and Yadav (1998) for dispersion of pollutants from a point source under stable conditions with light winds (Table 1). Zhu and Hinds (2005) modified the K-theory model for a line source to explain the decay of a freeway plume during daytime. The K-theory model yielded poorer fits to our nocturnal observations in the far downwind areas compared to the Gaussian model with a fitted Briggs formulation for σ_z.

The Briggs expression has slightly different formulations for rural and urban conditions (Table 1), the choice of which affects one of the two dispersion coefficients (β). Both forms fit the data equally well and produce nearly identical curve shapes. For three of our four transects, the best fit value for β is more consistent with the rural form (described more below). While this may seem surprising, much of Los Angeles, including these three transects, consist of single story residential development. The fourth transect, DTLA, has tall buildings in the area (although few tall buildings are on the transect itself; Supplement Sect. S1), and its β values are closer to expected urban values. Here, we use the rural form of the Briggs' formula as the basic equation for fitting the observations, to allow us to investigate meteorological and traffic effects on plume intensities and transport and compare them among the different sites. More discussion of the observed α and β are presented in Sect. 3.1.

$$\sigma_z(x) = \frac{\alpha \cdot x}{1 + \beta \cdot x} \tag{3}$$

Consequently, Eq. (2) combined with Eq. (3) was used to fit the observed data. This formulation, a semi-empirical Gaussian dispersion expression with an effective Briggs formulation (optimized by fitting observational data) is hereinafter referred to as the "semi-empirical GB model". Fitting with Eqs. (2) and (3) to observed concentration profiles was performed in a Matlab environment based on Matlab's built-in unconstrained nonlinear minimization of the sum of squared residuals (Lagarias et al., 1998). For better fitting results, the generalized Briggs values were used as an initial guess for the fit parameters.

We acknowledge that this semi-empirical GB model does not explicitly consider the traffic-related turbulence or surface roughness effects on dispersion. However, vehicle-induced turbulence is relatively short-lived, and has a dominant effect in the immediate vicinity of the roadways (Wang and Zhang, 2009; Gordon et al., 2012), becoming negligible within 60 m downwind from the roadways (Gordon et al., 2012). This range covers only a small fraction of our UFP profile range (up to 2 km). In addition, vehicle-induced turbulence likely varies little between our sampling sites and over our measurement time periods, for two reasons. First, because trucks and passenger cars induce markedly different turbulence, significant differences in vehicle fleets could result in differences in turbulence. In our study, however, diesel trucks consistently contributed less than 6 % of the total traffic for all freeways. Second, for the pre-sunrise periods, vehicle speeds are consistent among all sampling days and sites due to the consistent free-flow of traffic. As described in Supplement Sect. S1, all sites investigated had similarly built environments (i.e., transects were surrounded mostly with one-story residential single-family homes). Thus, we believe the surface roughness should be similar among our sampling sites.

Although particle number concentrations are influenced by particle dynamics such as coagulation, deposition, and condensation/evaporation, a common conclusion from previous studies is that dilution is the most important process controlling particle number (e.g., Kumar et al., 2011; Zhang et al., 2004; Jacobson and Seinfeld, 2004). Particularly near emission sources, such as the curbside of a major road, the dilution timescale is approximately one to two orders of magnitude faster than deposition and coagulation, respectively (Kumar et al., 2011). Even under stable nocturnal conditions, dilution appears to be the most important sink accounting for ~ 70 % of the overall decay rates (Choi and Paulson, 2014). Nonetheless, we note that dispersion parameter β (as discussed in Sect. 3.1) represents additional UFP number losses besides dilution/dispersion due to these transformation processes because here dispersion parameters (α and β) were extracted by fitting the observed UFP profiles of the "real" atmosphere. Thus, the use of dispersion parameters determined in the present study should be made with the caution that a model including a particle dynamics module explicitly is likely to double-count particle transformation effects. We believe, nonetheless, this is another advantage of our analytical approach, because current dispersion models have been developed initially based on non-reactive conservative species, and particle dynamics are not yet perfectly captured in models (Zhang et al., 2004; Jacobson and Seinfeld, 2004).

2.3.2 Semi-empirical GB Model fitting parameters (Q_c, α, and β)

The semi-empirical GB model, a combination of an analytical solution for Gaussian dispersion and undetermined Briggs formulation, includes three free variables, the emission parameter Q_c and two dispersion parameters α and β (Eqs. 2 and 3). These variables are to be determined by fitting to the observed concentration profiles. Thus, in this section, we examine how these unknown variables (Q_c, α and β) are influenced by the spatial distribution of UFP concentrations. In this way, if the semi-empirical GB model explains the observed concentration profiles well (Sect. 3.1) we can infer which factors control the plume parameters in the semi-empirical GB model (Sect. 3.2), verify these hypothesized relationships based on the observations (Sects. 3.3 and 3.4), and consequently derive predictive equations for plume parameters (Sect. 3.6).

In advance of further discussion concerning the variations of plume parameters with respect to observed concentration profiles, it is worth examining if the three plume parameters have built-in relationships among one another in the fitting function itself, prior to relating the variations in plume parameters to physical processes and meteorological parameters. As discussed in more detail in Supplement Sect. S4, Q_c, the wind-corrected emission factor is independent of the distance from the freeway (x), while the influence of α and β on the calculated concentration both depend directly on x. For a given intersection geometry, the magnitude of Q_c determines the peak concentration, and the overall magnitude of the curve, with no relation to α and β. Note, α and β have dominant effects on the shape of the decay curve close to the peak and at long distances, respectively (Figs. 2 and S3b and c in Supplement Sect. S4). Empirically they exhibit linear relationships to each other (Fig. 3 and discussions below), but these empirical relationships cannot be predicted a priori from Eq. (2), and further evidently depend on the transect–freeway intersection geometry. As a result, they cannot be used in turn to reduce the number of variables in Eq. (2). In summary, the relationships between Q_c, α and β, where observed (see below), appear to result from the fact that they respond to many of the meteorological variables in ways that overlap.

The emission parameter Q_c, which represents the wind speed-corrected emission factor, influences only the magnitude of the peak and the overall pollutant concentrations. With fixed α and β, varying Q_c does not change the decay curves once they are normalized with the peak concentrations. Thus, this approach allows us to estimate an emission factor for a mixed vehicle fleet on major roads directly from the observed concentration profiles. The details of this analysis are discussed in Sect. 3.5.

Plume shape includes both the location of the concentration peak and its decay shape. It is instructive to examine the relationships between α and β and plume shape: pollutant profiles simulated with Eqs. (2) and (3) clearly show that smaller α, holding β constant, corresponds to a freeway plume peak that appears farther downwind (Fig. 1a). With fixed α, decreasing β corresponds to a more rapid decrease in plume concentrations, but the peak location is unaffected (Fig. 1b). Here, we explore the values for α and β derived by fitting Eqs. (2) and (3) to the daily average profiles for the pre-sunrise sampling periods, in order to quantitatively investigate the effects of both meteorology and traffic density on the magnitude of peak concentrations and decay rates of freeway plumes (Table 2). If α and β can be properly parameterized with measurable properties such as surface meteorology, it will be possible to predict how widely freeway plumes influence vehicle-related pollutant concentrations in neighborhoods downwind of freeways under stable atmospheric conditions.

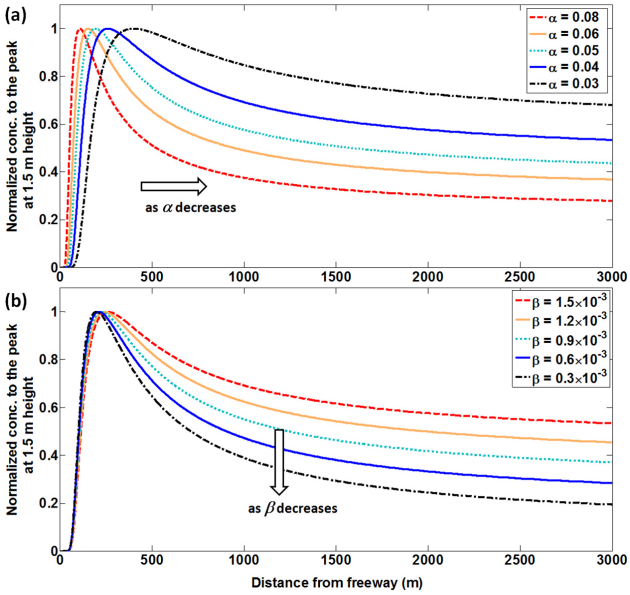

Figure 1. Variations in spatial profiles of pollutants calculated with Eqs. (2) and (3) varying α or β. The x axis is distance downwind from freeway and y axis is normalized concentrations to the peak at 1.5 m height ($z = 1.5$ m). Results were obtained **(a)** with fixed Q_c and $\beta = 1.5 \times 10^{-3}$ and varying α from 0.03 to 0.08, and **(b)** with a fixed Q_c and $\alpha = 0.04$, changing β from 0.3 to 1.5×10^{-3}.

Peak concentrations can be directly influenced by vehicle number and type (and other characteristics), passing on the freeway at the moment when the MMP crosses under or over the freeway, whereas the long early-morning plume tails result from rather slow transport. For example, with consistent winds of 0.5 m s^{-1}, air travel time is about 30 s and 1 h, respectively, at 15 m and 2 km downwind of freeway. Thus, an individual plume profile obtained by a single scan requiring 10 to 15 min of MMP driving is complicated to interpret. This is not only due to different timescales between the peak and tails of plumes; it is also due to the uneven traffic flows and composition at the moment when the MMP

crosses the freeways, which result in significantly varying plume peak concentrations of individual profiles. To minimize these effects, we use the daily average concentration profiles for pre-sunrise measurement periods. The one exception is Sect. 3.1 where median concentration profiles for all measurement days at each transect/site were fitted with the semi-empirical GB model for the comparisons with categorized Briggs values.

We note that the real-world problem addressed here is more complex than the simple case of dispersion from a steady line source. While UFP are a very good tracer for roadway pollutants, they do undergo a modest amount of coagulation and evaporation/condensation on the timescales of interest here. Further, the line source is not steady; in the early morning the traffic density increases rapidly with time. Finally, the geometry of the intersection of the transect and the freeway varies among locations. The α and β values extracted as part of the semi-empirical treatment presented here account for all of these effects. Full theoretical treatments of all of the details of this problem are beyond the scope of this paper.

3 Results and discussions

3.1 Effectiveness of the fit of the semi-empirical GB model to the observations and comparisons with generalized Briggs' parameterization

For all four transects, the fitted semi-empirical GB model provided excellent matches to the observed profiles of UFP number concentrations both at the peak and far downwind ($R^2 \sim 0.9$ or better) (Fig. 2). This implies that the three plume parameters (Q_c, α and β) can be estimated correctly from related explanatory variables, and the plume shape and length, including the peak and far downwind concentrations, can be described well. In addition, simple plume parameters make straightforward and quantitative the complicated links between dispersion/transport of freeway pollutant plumes and meteorological, traffic and geographical conditions. The fits do not explain slightly elevated UFP concentrations immediately upwind of the freeways. These elevations likely result from a combination of wind variability on a short timescale (or meandering behavior under calm conditions) and eddy diffusion in the direction opposite to the prevailing winds, neither of which is captured in the model.

Comparing α and β values, which were obtained from the median concentration profiles for each site (all days combined) (Fig. 2), with conventional Briggs expression provides an overview of how well the transects are described by the simple expression of dispersion parameters provided by Briggs and other similar formulations. Day-to-day variability (based on daily averaged concentration profiles) is discussed in the sections that follow. The mean values for α obtained from the transect-averaged UFP profiles were 0.07,

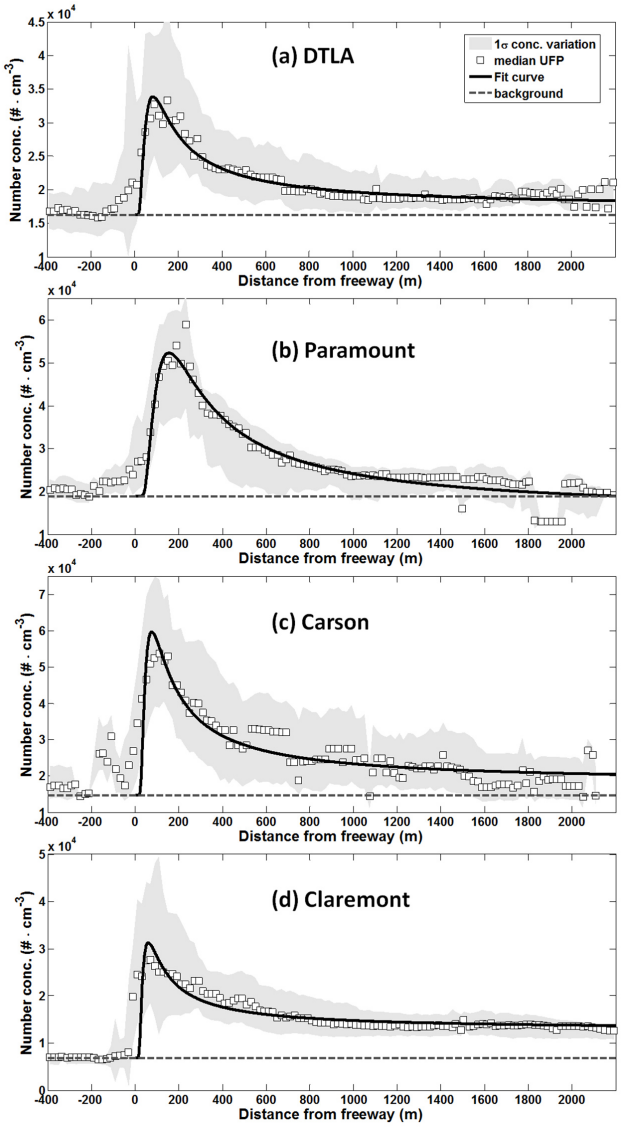

Figure 2. Observed median UFP number concentrations with distance downwind of freeways (white squares), 1σ variation ranges (gray areas), upwind background concentrations (horizontal gray dashed lines), and the semi-empirical GB model fits to the observations (black lines) for transects at **(a)** DTLA, **(b)** Paramount, **(c)** Carson, and **(d)** Claremont.

0.03, 0.02, and 0.03 for the DTLA, Paramount, Carson, and Claremont transects, respectively (Table 1). Briggs (1973) values for α and β are also listed in Table 1. The mean α for the DTLA transect (0.07) is similar to the Briggs' value for urban areas under stable conditions ($\alpha = 0.08$), whereas α for the other three transects are comparable to the Briggs' constant for rural areas under moderately to slightly stable conditions ($\alpha = 0.02$ to 0.03). It is however, not clear that the variations in α should be attributed to differences in land use because the immediate area surrounding the DTLA transect is also surrounded with low one- or two-story homes, similar

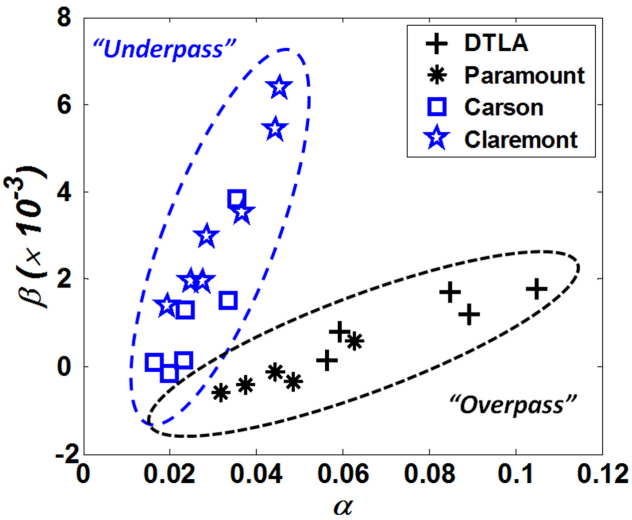

Figure 3. Relationship between α and β obtained from the fits of the semi-empirical GB model to the daily mean spatial profiles of UFP in the DTLA (black crosses), Paramount (black asterisks), Carson (blue squares), and Claremont (blue stars) transects. Black dotted line represents overpass freeway transects, where freeways overpass the transects, and blue dashed line underpass freeway transects, where freeways pass under the transects.

to the other transects. Large differences in α were observed for different freeways geometries (discussed in Sect. 3.2), and this may explain the higher α at the DTLA site.

The observed mean β values were 0.4×10^{-3}, -0.5×10^{-3}, 0.6×10^{-3}, and 2.8×10^{-3} for DTLA, Paramount, Carson, and Claremont, respectively (Table 1). These show larger differences from the Briggs' β value than was the case for α. The mean β for the DTLA and Paramount transects were smaller than the Briggs' value for urban (1.5×10^{-3}) and rural areas (0.3×10^{-3}), respectively (if the urban version of Briggs' formula was used, $\beta = 1.1 \times 10^{-3}$ was obtained for DTLA). In contrast, β observed in Claremont was higher than the Briggs' β value. The Carson transect yielded a slightly higher β than Briggs' β value. Physically, these results suggest UFP emitted from freeways passing over the MMP transect (DTLA & Paramount) dispersed more quickly than anticipated by the Briggs (1973) analysis, while for Claremont they dispersed more slowly.

Overall, the wide variations in both α and β by location when compared to the generalized Briggs' formula underline the generalized Briggs expression for σ_z is not sufficient, even under stable conditions. Those differences might be caused in part by freeway topographic features, particle dynamic losses such as coagulation and evaporation, as well as (particularly for β) rapid temporal traffic changes during pre-sunrise periods. The observed profiles are expected to have lower β compared to those for constant emission sources. For DTLA and Paramount where β was significantly lower than the Briggs' value, traffic increases from 1 h before the measurement period to the middle of the measurement period were significantly larger than those in Carson and Claremont (574 and 649 vehicles 5 min^{-1} for DTLA and Paramount vs. 384 and 292 vehicles 5 min^{-1} for Carson and Claremont, respectively). Despite the effects of emission changes on fitted β variations, β from observed profiles for the pre-sunrise period can still provide meaningful insights into atmospheric parameters controlling plume shape because (1) traffic variations and corresponding ambient UFP profiles are typical for those periods; (2) traffic flow changes are very consistent ($1\sigma < 10\,\%$) among weekdays, thus the effects of weekday emission changes should be consistent from day to day; (3) concentrations farther downwind in plumes are the least influenced by emissions from freeways because they get close to background levels due to the dilution processes; and (4) although it is implicit, additional loss processes due to particle dynamics are considered in β. As far as we are aware, these loss processes are not considered perfectly in current dispersion models applied to the real atmosphere. In any case, the model fitting methods provide an effective tool to estimate dispersion coefficients directly from the observations.

3.2 Impacts of dispersion coefficients and freeway-street interchange geometry on plume shapes

The dispersion coefficients α and β obtained from daily average concentration profiles for the pre-sunrise periods show a strong positive correlation with one another, but clearly fall into two exclusive groups, apparently the result of the freeway-street interchange geometry (Fig. 3). Inputs in the semi-empirical Gaussian equation (Eq. 2) for the two cases differ: source height $H = 6$ m for overpass freeway transects (freeway above transect) and $H = 0$ m for underpass freeway transects (freeway below transect). Compared to underpass freeway transects, α values for overpass freeways ranged more widely and β varied less. For overpass freeway transects, it takes more time for the vehicular plume to reach the ground from the elevated freeway height, thus the location of the peak, which depends on α, may vary depending on topographic and atmospheric conditions. In contrast, for underpass freeway transects, the peak will appear adjacent to the freeway regardless of atmospheric conditions because a plume rises directly from the freeway beneath, leading to smaller variations in α, and relatively larger variations in β.

The positive correlations between α and β suggest overlap in the factors that control them. Figure 1 illustrates that α is related to the peak position and plume width (advection), and β to plume dilution rates (eddy diffusion or entrainment). We can therefore hypothesize that the correlation between α and β is caused by (1) different wind conditions (advection and turbulence; hypothesis 1) and/or (2) the concentration difference between plume and background (plume intensity;

hypothesis 2). In the following sections, these two hypotheses are explored in detail.

3.3 Wind effects on plume characteristics (hypothesis 1: advection and dispersion)

The role of wind speed in the semi-empirical GB model is only to adjust the overall magnitude of concentrations (Eq. 1). Therefore, concentration profiles normalized to the peak concentration should have the same shape regardless of wind speed. In the real atmosphere, however, different wind conditions will produce different advection and dispersion behavior of pollutants, and thus wind effects contribute to variations in α and β. For example, higher wind speed is expected to transport the freeway plumes, which will manifest as decreasing α (Fig. 1a). At the same time, wind speeds are related to mechanical turbulence in the surface layer, which is the most important determinant for eddy diffusion in the absence of buoyancy forces, as is the case for pre-sunrise periods. Thus, higher wind speed is expected to produce more turbulence due to stronger wind shear, and also deepen the mechanical mixing length. This will disperse pollutants more rapidly, resulting in lower β values (Fig. 1b). Consequently, Hypothesis 1 attributes the positive correlation between α and β to wind speed variations under stable conditions. We note that the semi-empirical GB model assumes perpendicular winds and hence the changes in wind direction can also affect α values (particularly). Parallel winds result in higher α, while perpendicular winds which can transport plumes more effectively, resulting in decreasing α (Fig. 1a) compared to parallel winds. In the following sub-sections, we attempt to explain/verify this hypothesis by quantitatively comparing α and β with observed winds.

3.3.1 Wind direction

As expected, in addition to determining which side of a freeway is downwind, wind direction was a determinant of plume length. The dispersion coefficient α generally showed a negative relationship with wind direction (relative to the freeway; WD_{rel}, 90° = normal to freeway), suggesting as expected that plumes are more effectively transported if winds are perpendicular to the freeway (Fig. 4a). A positive correlation between $\Delta[UFP]_{1\,km}$, the background-subtracted UFP number concentration measured 1km downwind of the freeway ($[UFP]_{1\,km} - [UFP]_{bkgnd}$) and WD_{rel} illustrates the effects of WD_{rel} on plume transport (Fig. 4b). However, the high scatter indicates the importance of other factors. The dispersion coefficient β is not correlated with WD_{rel} (not shown), because wind direction is not directly related to the dilution process.

3.3.2 Wind speed

At night, statically stable air suppresses turbulent energy production, thus under calm stable conditions, moderate consistent winds can help transport an air mass farther. Hypothesis 1 suggests that both α and β would decrease (more transport and faster dispersion) as wind speeds increase under calm conditions, assuming a consistent wind direction. α is likely to be more related to vector-averaged resultant wind speeds because the hypothesis concerns transport, whereas β should depend more on scalar wind speed, which should most directly affect dispersion rates.

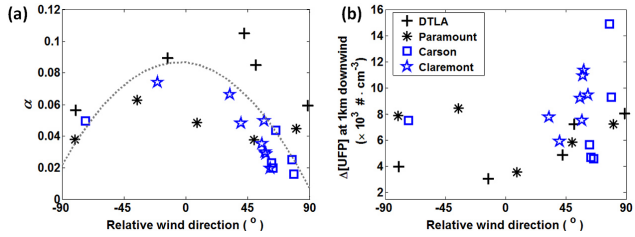

Figure 4. Wind direction effects on **(a)** dispersion coefficient, α, and **(b)** plume intensity (Δ[UFP]) at 1 km, which is defined as background-subtracted UFP concentrations at 1 km downwind of freeway. Black crosses, black asterisks, blue squares, and blue stars represent daily mean values for the DTLA, Paramount, Carson, and Claremont transects, respectively. Relative wind direction is daily mean wind direction relative to freeway orientation (90° = normal to freeway). Gray dotted line in **(a)** represents 2nd order polynomial fits ($R^2 = 0.48$).

Figure 5a shows that α responds differently to resultant wind speeds (WSR), depending on freeway–street interchange geometry. Clear negative relationships between α and resultant wind speeds (WSR) were observed for the overpass freeway transects (DTLA and Paramount, Fig. 5a). Different scales of α in DTLA and Paramount are not explained by wind speeds, but could result from factors such as plume intensities caused by different traffic densities, discussed below. Plumes emitted from the freeways above transects will be transported farther with higher resultant wind speeds before reaching the ground (smaller α), explaining the negative correlation between α and resultant wind speeds. In contrast, for the underpass freeways (Carson and Claremont), α appears to slightly increase with resultant wind speed, although the trend is largely driven by one data point obtained on 8 June 2011 (Fig. 5a). On that day, winds were unusually strong, the prevailing wind direction was reversed, and a fog formed in the downwind uphill area. For the underpass freeway transects, the peak concentration location might not be significantly influenced by wind speeds, since the MMP experienced a freshly emitted plume rising directly beneath the transect. Therefore, wind speeds might more strongly impact the dissipation rate (β) of a plume, creating faster decays and narrower peaks as the wind speed increases (Fig. 5b).

Scalar wind speeds (WSS) and β were, in general, negatively correlated when wind speeds were larger than $0.5\,m\,s^{-1}$, particularly for the underpass freeways (Fig. 5b). In contrast to the α-WSR relationships, the overpass freeway

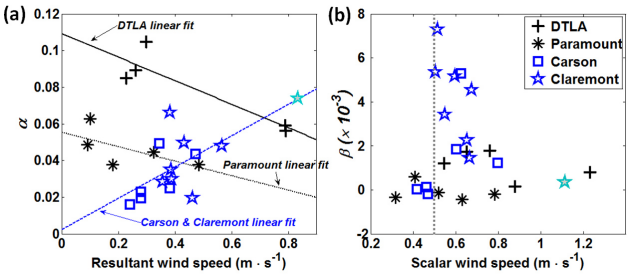

Figure 5. Variations in dispersion coefficients as a function of wind speed. **(a)** α vs. vector-averaged resultant wind speeds. **(b)** β vs. scalar-averaged wind speeds. Black solid line is a linear fit for the DTLA data points, black dotted line for Paramount, and blue dash-dotted line for Carson and Claremont. Vertical dotted line in **(b)** represents scalar wind speed of $0.5\,\mathrm{m\,s^{-1}}$. Light blue star denotes Claremont data obtained on 8 June 2011 when wind was strong with reversed prevailing wind direction and fogs in the uphill downwind area.

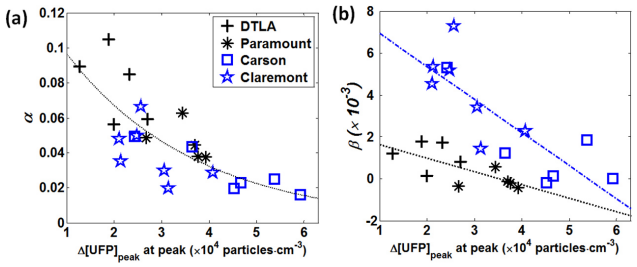

Figure 6. Plots of the relationships of concentration gradient ($\Delta[\mathrm{UFP}]_{\mathrm{peak}}$) at the peak with **(a)** α and **(b)** β. Dotted line in plot **(a)** is an exponential curve fit: $\alpha = 0.14 \cdot \exp(-3.64 \times 10^{-5} \cdot \Delta[\mathrm{UFP}]_{\mathrm{peak}})$ ($R^2 = 0.59$). Black dotted line and blue dash-dotted line in plot **(b)** are linear fits for overpass ($R^2 = 0.63$) and underpass ($R^2 = 0.67$) freeway transects, respectively.

transects were more weakly correlated than underpass freeway sites. It appears that wind speeds influence α more strongly for the overpass freeway transects, whereas for the underpass freeway transects β is more affected by wind speeds. This negative correlation is not valid under extremely light wind conditions (WSS $< 0.5\,\mathrm{m\,s^{-1}}$). Under these calm stable conditions, other parameters are likely to govern the dilution rate of a plume, such as the concentration gradient (Sect. 3.4). Overall, within the small range of wind speed observed in early morning, winds alone are not the dominant factor in determining dispersion coefficients α and β under stable pre-sunrise conditions. Consequently, hypothesis 1 by itself cannot entirely explain the variations in plume decays.

3.4 Effects of freeway emissions on plume extension (hypothesis 2)

In the analytical solution of Gaussian dispersion (Eq. 2), the emission factor Q_{c} is not directly related to plume decays, transport, α or β (Sect. 2.3.2 and Supplement Sect. S4). Considering that the increase in wind speeds reduces Q_{c} (Eqs. 1 and 2) if emission rates are constant, and at the same time, increased wind speeds are likely linked with decreased α and β (through effective transport and faster dissipation; Hypothesis 1), positive correlations between Q_{c} vs. α and β might be expected. In Fig. 6, however, we found strong negative correlations between Q_{c} and plume dispersion parameters α and β (Q_{c} was determined by fitting the background-subtracted peak concentration, or "plume intensity" $\Delta[\mathrm{UFP}]_{\mathrm{peak}}$). Thus, observed negative correlations imply that winds may not be a dominant factor controlling plume shapes under stable conditions with low winds ($< 1\,\mathrm{m\,s^{-1}}$). Hypothesis 2 states that plume decay rates are a function of concentration differences between plumes and backgrounds ($\Delta[\mathrm{UFP}]$): as $\Delta[\mathrm{UFP}]$ becomes larger, concentration decreases faster with downwind distance. These relationships are clearly shown in Fig. 6.

3.4.1 Effects of Δ[UFP] on plume decay rates

The plume intensity parameter $\Delta[\mathrm{UFP}]_{\mathrm{peak}}$, defined as the difference between the background and plume peak concentration, showed clear and consistent negative correlations with both the dispersion coefficients α and β (Fig. 6a and b), in contrast to its positive correlations with wind speed and direction. Although α and $\Delta[\mathrm{UFP}]_{\mathrm{peak}}$ seem to follow a single trend line, the transects populate different parts of the curve, with larger $\Delta[\mathrm{UFP}]_{\mathrm{peak}}$ corresponding to the underpass freeway transects. Due to different slopes in these two groups, the overall trend line has an exponential form ($\alpha = 0.14 \cdot \exp(-3.64 \times 10^{-5} \Delta[\mathrm{UFP}])$, $R^2 = 0.59$), however this appears to arise from the presence of two distinct populations; these are also observed in comparisons of α and β with explanatory parameters such as wind speeds, $\Delta[\mathrm{UFP}]_{\mathrm{peak}}$ and Q_{c} (Figs. 3, 5, 6a and 9b). Dependencies of β on $\Delta[\mathrm{UFP}]_{\mathrm{peak}}$ fall into two groups corresponding to freeway–street interchange geometry, as discussed in Sect. 3.2 (Fig. 6b). The negative correlation between β and $\Delta[\mathrm{UFP}]_{\mathrm{peak}}$ is consistent with hypothesis 2, as β appears to be a parameter related to plume dissipation (Sect. 2.3.2, Fig. 1b). For these reasons, we conclude the decay rates are strongly influenced by not only wind speed and direction but also the concentration difference relative to the background, that is, $\Delta[\mathrm{UFP}]_{\mathrm{peak}}$.

Let us consider a simple first-order Lagrangian expression for dilution and particle dynamics processes rates during the freeway plume transport (Eq. 4), similar to the expression used in some urban plume transport models (Dillon et al.,

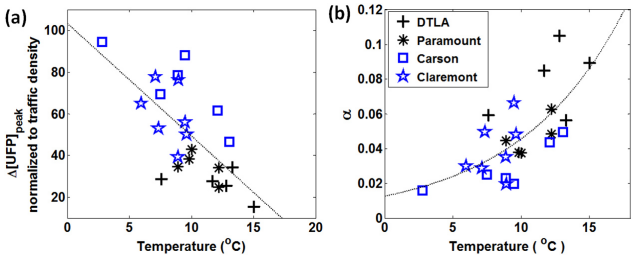

Figure 7. Temperature effects on **(a)** peak concentration difference from the background ($\Delta[\mathrm{UFP}]_{\mathrm{peak}} = [\mathrm{UFP}]_{\mathrm{peak}} - \mathrm{background}$ $[\mathrm{UFP}]_{\mathrm{bkgnd}}$) normalized to traffic density and **(b)** dispersion coefficient α. Black dotted lines are curve fits: **(a)** $\Delta[\mathrm{UFP}]_{\mathrm{peak}} \cdot (\mathrm{Traffic})^{-1} = -5.41 \cdot T + 103.4$ $(R^2 = 0.46)$ and **(b)** $\alpha = 1.27 \times 10^{-2} \cdot e^{0.13} \cdot T$ $(R^2 = 0.48)$.

2002; LaFranchi et al., 2011):

$$\frac{\mathrm{d}\left([C]_t - [C]_{\mathrm{bkgnd}}\right)}{\mathrm{d}t} = -\left(K_{\mathrm{dilution}} + K_{\mathrm{coagulation}} + K_{\mathrm{deposition}} + K_{\mathrm{evaporation}}\right) \cdot \left([C]_t - [C]_{\mathrm{bkgnd}}\right) \quad (4)$$

$$[C]_t - [C]_{\mathrm{bkgnd}} = \left([C]_{\mathrm{peak}} - [C]_{\mathrm{bkgnd}}\right) \cdot \exp\left(-\left(K_{\mathrm{dilution}} + K_{\mathrm{coagulation}} + K_{\mathrm{deposition}} + K_{\mathrm{evaporation}}\right) \cdot t\right), \quad (5)$$

where t is time, $[C]_t$ and $[C]_{\mathrm{bkgnd}}$ are pollutant concentrations at time t in the plume and in the background, respectively, and K represents first-order decay rate coefficient for each particle loss process: dilution, coagulation, dry deposition and evaporation. If we assume Ks are constant for an hour (corresponding to 1 to 2 km of plume transport), the solution of Eq. (4) shows $\Delta[\mathrm{UFP}]_{\mathrm{peak}}$ is independent of plume decay (loss) rates when the plume concentrations are normalized (Eq. 5). We note that the above expression only deals with β because the concentration at $t = 0$ is considered as the peak concentration. Consequently, we concluded additional loss rates due to particle transformation are not attributed to the observed clear relationships between $\Delta[\mathrm{UFP}]_{\mathrm{peak}}$ and β (Fig. 6b).

The rapid increase in traffic flows during pre-sunrise measurement periods for morning commutes likely explains the negative correlation between $\Delta[\mathrm{UFP}]_{\mathrm{peak}}$ and β (as discussed in Sect. 2.3.2). The peak concentration is instantly affected by the emissions from freeway traffic, whereas far downwind concentrations result from the emissions in the past when an air mass passed over the freeway, as well as the background concentration at that time. Thus, the temporal variations of far downwind concentrations should be relatively smaller and less rapid than those near the peak concentrations. These patterns are clearly observed in the 1σ variation ranges of the average concentration profiles shown in Fig. 2. For the morning commute periods, increasing emissions from corresponding traffic flows produce larger $\Delta[\mathrm{UFP}]_{\mathrm{peak}}$ but these emission increases do not instantly alter the far downwind concentrations, amplifying concentration decreases with distance (and lowering β).

However, the above discussions concern the relationships of $\Delta[\mathrm{UFP}]_{\mathrm{peak}}$ with β. If or why $\Delta[\mathrm{UFP}]_{\mathrm{peak}}$ controls α is not clear. It is possible that α and β are related to each other due likely to hypothesis 1 and $\Delta[\mathrm{UFP}]_{\mathrm{peak}}$ intensifies β variation while not altering the relationships between α and β, leaving a negative correlation between $\Delta[\mathrm{UFP}]_{\mathrm{peak}}$ and α. Alternatively, it is also possible that $\Delta[\mathrm{UFP}]_{\mathrm{peak}}$ directly determines α given that lower α values tend to correspond to increases in the overall magnitude of concentrations of the profiles (Fig. 1a), explaining the negative correlation between α and $\Delta[\mathrm{UFP}]_{\mathrm{peak}}$. Despite these incomplete discussions of the underlying causation, it is clear that plume intensities $\Delta[\mathrm{UFP}]_{\mathrm{peak}}$ show strong negative correlations with α and β.

3.4.2 Temperature, atmospheric stability, and emission factor

Although temperature does not directly affect the dissipation rates of plumes, we found a clear positive correlation between the temperature and the dispersion coefficient, α (Fig. 7b). Because higher UFP emissions from vehicle tailpipes are strongly related to colder temperatures, particularly for the nucleation mode (10–20 nm) (Kittelson et al., 2001, 2004; Morawska et al., 2005), colder temperatures might indirectly lower dispersion coefficients by elevating UFP concentrations from vehicular sources, and hence increasing $\Delta[\mathrm{UFP}]_{\mathrm{peak}}$ (Fig. 6a). Consistent with this explanation and supporting the emissions studies (Kittelson et al., 2001, 2004; Morawska et al., 2005), $\Delta[\mathrm{UFP}]_{\mathrm{peak}}$ values normalized to the traffic density, indeed, increase as ambient temperatures decrease for all transects (Fig. 7b). Zhu et al. (2006) also showed the same inverse relationship between temperature and UFP concentrations corrected for traffic volume at the edge of the I-405 freeway.

The Richardson number (R_i) is a common indicator of atmospheric stability. It combines the vertical temperature gradient (static stability) with mechanical wind shear (Stull, 1988) as expressed in Eq. (6):

$$\text{Richardson number,}\ R_i \equiv \frac{g}{\overline{\theta}} \frac{\mathrm{d}\theta}{\mathrm{d}z} \cdot \left(\frac{\mathrm{d}U}{\mathrm{d}z}\right)^{-2}, \quad (6)$$

where $\overline{\theta}$ is the mean potential temperature in the layer, $\mathrm{d}\theta \cdot \mathrm{d}z^{-1}$ is temperature gradient, $\mathrm{d}U \cdot \mathrm{d}z^{-1}$ is vertical wind shear, and g is the gravitational acceleration ($R_i > 0$ for stable; $R_i = 0$ for neutral; and $R_i < 0$ for unstable air). R_i values for all transects fell in the near-neutral to stable ranges during the pre-sunrise periods (Fig. 8). Background UFP concentrations tend to increase when air is more stable (Fig. 8a), as expected. However, the decay rate coefficient β appears to decrease (the plume dissipates more rapidly) when the nocturnal atmosphere is more stable (Fig. 8b). We interpret this phenomenon as a result of hypothesis 2; under stable conditions, $\Delta[\mathrm{UFP}]_{\mathrm{peak}}$ tends to increase, leading to a fast concentration decay rate in a plume as discussed above.

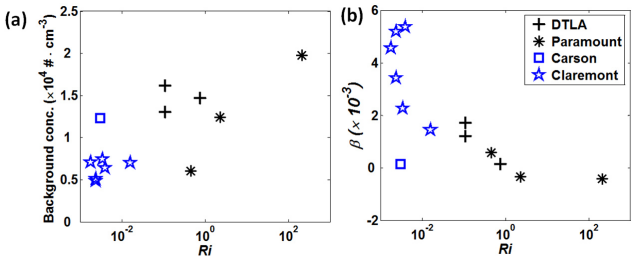

Figure 8. Dependence of **(a)** background UFP concentrations and **(b)** dispersion coefficient, β on atmospheric stability, represented by the Richardson number (R_i).

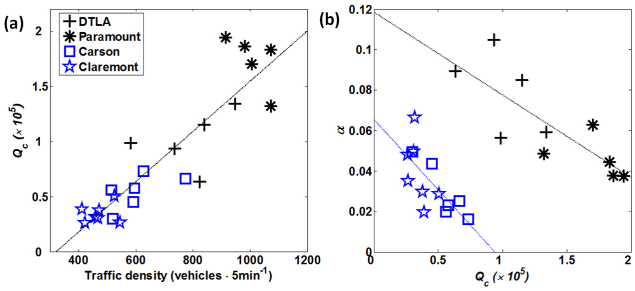

Figure 9. (a) Emission parameter, Q_c as a function of traffic density (vehicles 5 min^{-1}) in four sampling sites, and **(b)** α variations as a function of Q_c. Dotted line represents a linear fit to all data points in the plot: **(a)** $Q_c = 227.7 \times$ (Traffic flow) $- 7.3 \times 10^4$ ($R^2 = 0.80$) and **(b)** $\alpha = -4.1 \times 10^{-7} \cdot Q_c + 0.12$ ($R^2 = 0.63$ for overpass freeways) and $\alpha =$ -6.9 $\times 10^{-7} \cdot Q_c + 0.065$ ($R^2 = 0.51$ for underpass freeways).

Consequently, the effects of temperature and atmospheric stability on plume dissipation rates further support the importance of hypothesis 2 for plume decay rates. Nonetheless, we should emphasize that faster decay rates do not necessarily mean reduced plume impacts because faster dissipations were observed for higher $\Delta[\mathrm{UFP}]_{\mathrm{peak}}$ conditions, and higher peak concentrations eventually lead to more elevated UPF concentrations in the far downwind areas (e.g., $\Delta[\mathrm{UFP}]_{\mathrm{peak}}$ shows a positive correlation with $\Delta[\mathrm{UFP}]$ at 1500 m downwind from the freeway; not shown).

3.5 Estimate of particle number emission factor

Vehicular emissions from the freeways depend on traffic volumes, fleet composition and maintenance, driving conditions, and fuel composition (e.g., sulfur content) (Kumar et al., 2011). Emission rates of UFP estimated by a number of previous studies show considerable variability (Kumar et al., 2011). The freeways studied here have similar vehicle composition with modest contributions from heavy-duty vehicles (< 3 to 6 %), and consistent traffic speeds due to lower traffic densities during the pre-sunrise periods. Thus, it is expected that traffic volume is a dominant factor in controlling the variations in emission rates from the freeways. Figure 9a shows a strong linear relationship between the emission parameter, Q_c and traffic density during the measurement periods, at least when traffic flow ranged from 400 to 1200 vehicles 5 min^{-1}, further supporting the effectiveness of the approach described here, including the ability of Q_c to describe vehicular emission rates from the freeways.

With the mean Q_c (8.12×10^4 particles m m^{-3}), observed wind speeds (0.64 m s^{-1}), a wind speed correction factor due to traffic wake suggested by Chock (1978) for stable air (0.2 m s^{-1}), and observed traffic flows on freeways (680 vehicles 5 min^{-1}), the mean particle number emission factor (PNEF), q_{veh}, can be estimated from Eq. (7):

$$q_{\mathrm{veh}} = \frac{\sqrt{2\pi}\, Q_c \cdot U_e}{(\text{traffic density})} = \frac{\sqrt{2\pi} \times \left(8.12 \times 10^4 \mathrm{m\,cm^{-3}}\right) \times (0.64 + 0.2\,\mathrm{m\,s^{-1}}) \times 10^6 \mathrm{cm^3 m^{-3}} \times 300\,\mathrm{s}\,5\,\mathrm{min^{-1}}}{\left(680\,\text{vehicles}\,5\,\mathrm{min^{-1}}\right)}, \quad (7)$$

where the last two values of the numerator are unit conversion factors. This estimate is for "survived" UFP through the very early stage of vigorous mixing/particle dynamics occurring within 1 to 3 s of initial emissions from tailpipes (Zhang and Wexler, 2004). The averaged q_{veh} for a mixed fleet on the 101, 91, I-110, and I-210 freeways with consistent fleet speeds under stable pre-sunrise conditions was estimated as 7.5(±0.4) $\times 10^{13}$ particles km^{-1} vehicle^{-1}, which is smaller than the estimate (5.2×10^{14} particles km^{-1} vehicle^{-1}) made in a similar manner by Zhu and Hinds (2005) for the nearby I-405 freeway in 2001. Although our PNEF estimate does not consider the initial stage on tailpipe-to-road scale (Zhang and Wexler, 2004), we note (1) the "survived" ultrafine particles can potentially affect human exposures and urban aerosol budgets on road-to-ambient scale and (2) ambient conditions under which measurements were conducted were representative of stable pre-sunrise periods generally found in the SoCAB with respect to traffic patterns/composition and surface meteorology. We also note the previous estimate made in 2001 (Zhu and Hinds, 2005) did not consider detailed particle dynamics, so that comparison between the two studies is appropriate.

In Choi et al. (2012), we also reported reduced peak UFP concentrations near freeways compared to the peak values observed in 2008 and 2005 by Hu et al. (2009) and Zhu et al. (2006), respectively. In addition, Quiros et al. (2013) reported a value of PNEF (3.7×10^{13} particles km^{-1} vehicle^{-1}) similar to our estimate. Between 2001 and 2010, many characteristics of the vehicle fleet have changed, such as improvement of engine emissions control technology, fleet turnover to newer cleaner vehicles, recent shifts to smaller engines (Snyder, 2011), and more stringent regulations for truck engines and fuel composition by the California Air Resources Board (CARB, 2004, 2008) as discussed in Quiros et al. (2013).

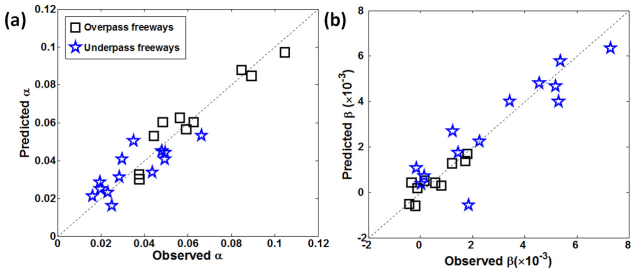

Figure 10. Comparisons of predicted dispersion coefficients **(a)** α ($R^2 = 0.88$) and **(b)** β ($R^2 = 0.86$) with the values extracted from observed concentration profiles. Black squares are for the overpass freeway transects (DTLA and Paramount) and blue stars for underpass freeways (Carson and Claremont). Dotted line represents 1:1 relationship.

3.6 Predicting plume behavior

Accurate prediction of plume peak heights and extents without the use of highly specialized data is clearly desirable. Our results suggest that the Gaussian line source model can accurately predict not only the peak concentration but also the extension of the plumes if we can properly estimate Q_c, α, and β (Eq. 2). Here, we use a multivariate linear regression (MVR) method to reproduce plume parameters (Q_c, α and β). Because plume peak concentration determined by Q_c is an important parameter controlling the dispersion coefficients α and β (Sect. 3.4.1), we found the best results by first estimating Q_c from various related factors, and then adding Q_c as a predictor variable in MVR analysis for α and β as discussed below.

For Q_c estimation, traffic flows, wind direction, wind speeds, temperature, and relative humidity were used as predictor variables based on theoretical and observed (measurement period average) relationships between ΔUFP and predictor variables (Eq. 8):

$$Q_{c,j} = \mathrm{coef}_1 \cdot \mathrm{TF}_j + \mathrm{coef}_2 \cdot \left|\mathrm{WD}_{\mathrm{rel},j}\right| + \mathrm{coef}_3 \cdot \mathrm{WSR}_j + \mathrm{coef}_4 \cdot T_j + \mathrm{coef}_5 \cdot \mathrm{RH}_j + C \quad (j = 1, 2, 3, \ldots, k), \tag{8}$$

where j indicates the jth observation, and TF, $\mathrm{WD}_{\mathrm{rel}}$, WSR, T, RH, and C are the traffic flows (vehicles $5\,\mathrm{min}^{-1}$), wind direction relative to the freeway orientation (°), ambient temperature (°C), resultant wind speed ($\mathrm{m\,s}^{-1}$), relative humidity (%), and a correction factor, respectively. Similarly, α (for overpass freeways) and β (for underpass freeways) were obtained from the observed meteorological and emission data (Q_c) (Eq. 9):

$$\alpha_j \text{ or } \beta_j = \mathrm{coef}_1 \cdot Q_{c,j} + \mathrm{coef}_2 \cdot \left|\mathrm{WD}_{rel,j}\right| + \mathrm{coef}_3 \cdot T_j + \mathrm{coef}_4 \cdot \mathrm{WSR}_j + \mathrm{coef}_5 \cdot \mathrm{RH}_j + C \quad (j = 1, 2, 3, \ldots, k). \tag{9}$$

In this analysis observed Q_c was used as an input parameter rather than estimated Q_c from Eq. (8) to avoid multivariate regression error. Regressions were performed separately according to freeway topography because as discussed earlier, α varied more widely for overpass freeways and β had a wider range for underpass freeways (Fig. 3). In addition, there were different dependencies of dispersion parameters on WSR and Q_c (Figs. 5a and 9b) for the two interchange geometries.

Calculated coefs, and resulting R^2 and p values for both Q_c, α and β are listed in Table 3. For Q_c, temperature and traffic were important parameters for both overpass and underpass freeways, while wind speed and wind direction were important only for overpass freeways and underpass freeways, respectively. The inverse sign for coef_1 (traffic flows) against observations was likely due to multicollinearity effects between predictor parameters (O'Brien, 2007). Although multicollinearity is detrimental to estimating the comparative importance of individual explanatory parameters, it does not reduce prediction validity or reliability of regression results as a whole (Lipovetsky and Conklin, 2001), The resulting Q_c from MVR showed good agreement with the values extracted from observations by fitting with overall R^2 of 0.95.

Dispersion coefficients were most sensitive to Q_c and least sensitive to T for both freeway geometries. Although RH by itself was poorly correlated with α and β, it showed modest importance in multivariate regressions. As noted, α and β showed strong positive correlations with one another, once separated for interchange geometry (Fig. 3; Eqs. 10 and 11):

$$\beta = 3.45 \times 10^{-2}\alpha - 1.64 \times 10^{-3} (R^2 = 0.90) \tag{10}$$

for overpass freeway transects

$$\alpha = 5.37\beta + 1.93 \times 10^{-2} (R^2 = 0.74) \tag{11}$$

for underpass freeway transects.

Thus, from appropriately estimated α or β from multivariate regressions, we could further obtain β or α using Eqs. (10) and (11). Overall, resulting values of α and β from multivariate regression analyses showed good agreement with the values extracted from observed concentration profiles by fitting, with $R^2 = 0.88$ and 0.86 for overpass and underpass freeways, respectively (Fig. 10). The evaluation of the MVR results is limited by the insufficient number of data used in training processes (13 for underpass freeways and 10 for overpass freeways). Nonetheless, the best estimates of uncertainties from the MVR analysis are ± 0.018 and ± 0.0018 for α and β, respectively. Independent error analysis also resulted in mean error estimates of 26 % for α and 60 % for β. More details about the evaluation processes are described in Supplement Sect. S5. Despite successful application of multivariate regression, we still note that input data points were not sufficient compared to the number of predictor variables in this multivariate regression analysis. Thus, further measurements are needed to verify these results.

Table 3. Coefficients for α (for overpass freeways) and β (for underpass freeways) obtained from multivariate linear regression using Eq. (8). Bold fonts represent the dominant contributors in the analyses.

	Emission factor Q_c		Dispersion coefficients	
	Overpass FWY (DTLA & Paramount)	Underpass FWY (Carson & Mountain)	α (Overpass FWY)	β (Underpass FWY)
coef1	-2.1×10^2	**55.7**	$\mathbf{-4.4 \times 10^{-7}}$	$\mathbf{-1.7 \times 10^{-7}}$
coef2	-5.8×10^2	$\mathbf{5.2 \times 10^2}$	3.5×10^{-4}	-8.7×10^{-5}
coef3	$\mathbf{-1.8 \times 10^5}$	-2.3×10^4	-3.3×10^{-2}	$\mathbf{-1.3 \times 10^{-2}}$
coef4	$\mathbf{-3.9 \times 10^4}$	$\mathbf{-1.2 \times 10^3}$	3.7×10^{-3}	-1.2×10^{-4}
coef5	-8.3×10^2	-31.7	$\mathbf{7.1 \times 10^{-4}}$	-8.1×10^{-5}
C	9.8×10^5	9.8×10^4	2.3×10^{-2}	2.8×10^{-2}
R^2	0.84 (0.092)	0.75 (0.042)	0.91 (0.032)	0.81 (0.018)
(p value)	Overall $R^2 = 0.95$			

Nonetheless, we consequently believe this approach provides an efficient and precise tool to predict freeway plume profiles near major roadways under stable conditions in that (1) dispersion parameters as well as particle number emission rates were extracted directly from the real atmosphere; (2) these simple dispersion parameters include particle transformation and traffic change effects in them and explain the observed UFP concentration profiles, producing excellent agreement for all sampling sites; (3) quantitative and straightforward comparisons between plume parameters and controlling meteorological/traffic factors suggest that winds were not the dominant factor to determining the plume shapes and downwind concentrations under stable pre-sunrise conditions; (4) elevated $\Delta[\mathrm{UFP}]_{\mathrm{peak}}$ from the onset of the morning commute in stable air appeared to be a more important factor for controlling the concentration decay rates with distance under considered conditions, which are difficult to represent even with the current comprehensive models, and hence should be considered more precisely in those models; (5) multivariate regression results can be applied with readily and routinely measurable variables without sophisticated model expertise to predict the peak concentration and its location as well as freeway plume impact areas under similar conditions with increasing traffic.

Although investigated environments were limited (nocturnal calm stable conditions with increasing traffic in residential areas) and hence our results are not expected to be directly applicable to other environments with different surface roughness and air stability, our results have potential implications given that many residential areas near freeways/highways have similarly built environments (at least in the US) and nocturnal stable conditions are common. Particularly we note that about 50 % of the population lives within 1.5 km of freeways in the South Coast Air Basin of California (Polidori et al., 2009). This study also has the potential to parameterize dispersion coefficients and emission factors for more sophisticated model simulations, providing clear UFP concentration profiles in a data set with a high spatial resolution under stable conditions, particularly for the onset of morning commute periods.

The Supplement related to this article is available online at doi:10.5194/acp-14-6925-2014-supplement.

Acknowledgements. The authors gratefully acknowledge support for this study by the California Air Resources Board, contract no. 09-357 and US National Science Foundation, contract no. CNS-1111971001. The mobile monitoring platform measurements were made possible with the generous assistance of our colleagues: M. He, K. Kozawa, S. Mara, and V. Barbesant. The authors appreciate the comments of two anonymous reviewers, helpful discussions with T. Callahan (University of Southern California), and especially the constructive criticism of the editor, which greatly improved the manuscript.

Edited by: R. MacKenzie

References

Briant, R., Korsakissok, I., and Seigneur, C.: An improved line source model for air pollutant dispersion from roadway traffic, Atmos. Environ., 45, 4099–4107, 2011.

Briggs, G. A.: Diffusion estimation for small emissions, NOAA, Oak Ridge, TN, 1973.

Capaldo, K. and Pandis, S.: Lifetimes of ultrafine diesel aerosol, Carnegie Mellon University, Pittsburgh, PA, 2001.

CARB: The California diesel fuel regulations, California Air Resources Board, Sacramento; http://www.arb.ca.gov/fuels/diesel/diesel.htm (last access: 5 December 2012), 2004.

CARB: Amendments to adopt more stringent emission standards for 2007 and subsequent model year new heavy-duty diesel engines, California Air Resources Board, Sacramento, 2008.

Chen, H., Bai, S., Eisinger, D., Niemeier, D., and Claggett, M.: Predicting near-road $PM_{2.5}$ concentrations: Comparative assessment of CALINE4, CAL3QHC, and AERMOD, Trans. Res. Record, 2123, 26–37, doi:10.3141/2123-04, 2009.

Chock, D. P.: Simple line-source model for dispersion near roadways, Atmos. Environ., 12, 823–829, 1978.

Choi, W. and Paulson, S. E.: Closing ultrafine particle number budget near major roadways under stable conditions: particle dynamics contributions to observed UFP decay rates with distance from the source, in preparation, 2014.

Choi, W., He, M., Barbesant, V., Kozawa, K. H., Mara, S., Winer, A. M., and Paulson, S. E.: Prevalence of wide area impacts downwind freeways under pre-sunrise stable atmospheric conditions, Atmos. Environ., 62, 318–327, doi:10.1016/j.atmosenv.2012.07.084, 2012.

Dillon, M. B., Lamanna, M. S., Schade, G. W., Goldstein, A. H., and Cohen, R. C.: Chemical evolution of the Sacramento urban plume: Transport and oxidation, J. Geophys. Res.-Atmos., 107, 4045, doi:10.1029/2001jd000969, 2002.

Gordon, M., Staebler, R. M., Liggio, J., Makar, P., Li, S.-M., Wentzell, J., Lu, G., Lee, P., and Brook, J. R.: Measurements of enhanced turbulent mixing near highways, J. Appl. Meteorol. Clim., 51, 1618–1632, doi:10.1175/JAMC-D-11-0190.1, 2012.

Gramotnev, G., Brown, R., Ristovski, Z., Hitchins, J., and Morawska, L.: Determination of average emission factors for vehicles on a busy road, Atmos. Environ., 37, 465–474, doi:10.1016/s1352-2310(02)00923-8, 2003.

Heist, D., Isakov, V., Perry, S., Snyder, M., Venkatram, A., Hood, C., Stocker, J., Carruthers, D., Arunachalam, S., and Owen, R. C.: Estimating near-road pollutant dispersion: A model intercomparison, Transport. Res. D-Tr. E., 25, 93–105, 2013.

Hoek, G., Boogaard, H., Knol, A., De Hartog, J., Slottje, P., Ayres, J. G., Borm, P., Brunekreef, B., Donaldson, K., Forastiere, F., Holgate, S., Kreyling, W. G., Nemery, B., Pekkanen, J., Stone, V., Wichmann, H. E., and Van der Sluijs, J.: Concentration response functions for ultrafine particles and all-cause mortality and hospital admissions: results of a European expert panel elicitation, Environ. Sci. Technol., 44, 476–482, doi:10.1021/es9021393, 2010.

Hu, S. S., Fruin, S., Kozawa, K., Mara, S., Paulson, S. E., and Winer, A. M.: A wide area of air pollutant impact downwind of a freeway during pre-sunrise hours, Atmos. Environ., 43, 2541–2549, doi:10.1016/j.atmosenv.2009.02.033, 2009.

Hussein, T., Karppinen, A., Kukkonen, J., Harkonen, J., Aalto, P. P., Hameri, K., Kerminen, V. M., and Kulmala, M.: Meteorological dependence of size-fractionated number concentrations of urban aerosol particles, Atmos. Environ., 40, 1427–1440, doi:10.1016/j.atmosenv.2005.10.061, 2006.

Jacobson, M. Z. and Seinfeld, J. H.: Evolution of nanoparticle size and mixing state near the point of emission, Atmos. Environ., 38, 1839–1850, doi:10.1016/j.atmosenv.2004.01.014, 2004.

Karner, A. A., Eisinger, D. S., and Niemeier, D. A.: Near-roadway air quality: synthesizing the findings from real-world data, Environ. Sci. Technol., 44, 5334–5344, doi:10.1021/es100008x, 2010.

Kerminen, V. M., Pakkanen, T. A., Makela, T., Hillamo, R. E., Sillanpaa, M., Ronkko, T., Virtanen, A., Keskinen, J., Pirjola, L., Hussein, T., and Hameri, K.: Development of particle number size distribution near a major road in Helsinki during an episodic inversion situation, Atmos. Environ., 41, 1759–1767, doi:10.1016/j.atmosenv.2006.10.026, 2007.

Kittelson, D. B., Watts, W. F., and Johnson, J. P.: Fine particle (nanoparticle) emissions on Minnesota Highways, Final Report, Minnesota Department of Transportation, 2001.

Kittelson, D. B., Watts, W. F., and Johnson, J. P.: Nanoparticle emissions on Minnesota highways, Atmos. Environ., 38, 9–19, doi:10.1016/j.atmosenv.2003.09.037, 2004.

Knol, A. B., de Hartog, J. J., Boogaard, H., Slottje, P., van der Sluijs, J. P., Lebret, E., Cassee, F. R., Wardekker, A., Ayres, J. G., Borm, P. J., Brunekreef, B., Donaldson, K., Forastiere, F., Holgate, S. T., Kreyling, W. G., Nemery, B., Pekkanen, J., Stone, V., Wichmann, H. E., and Hoek, G.: Expert elicitation on ultrafine particles: likelihood of health effects and causal pathways, Particle and Fibre Toxicology, 6, 19, doi:10.1186/1743-8977-6-19, 2009.

Kozawa, K. H., Fruin, S. A., and Winer, A. M.: Near-road air pollution impacts of goods movement in communities adjacent to the Ports of Los Angeles and Long Beach, Atmos. Environ., 43, 2960–2970, doi:10.1016/j.atmosenv.2009.02.042, 2009.

Kumar, P., Robins, A., Vardoulakis, S., and Britter, R.: A review of the characteristics of nanoparticles in the urban atmosphere and the prospects for developing regulatory controls, Atmos. Environ., 44, 5035–5052, doi:10.1016/j.atmosenv.2010.08.016, 2010.

Kumar, P., Ketzel, M., Vardoulakis, S., Pirjola, L., and Britter, R.: Dynamics and dispersion modelling of nanoparticles from road traffic in the urban atmospheric environment-A review, J. Aerosol. Sci., 42, 580–603, doi:10.1016/j.jaerosci.2011.06.001, 2011.

LaFranchi, B. W., Goldstein, A. H., and Cohen, R. C.: Observations of the temperature dependent response of ozone to NO_x reductions in the Sacramento, CA urban plume, Atmos. Chem. Phys., 11, 6945–6960, doi:10.5194/acp-11-6945-2011, 2011.

Lagarias, J. C., Reeds, J. A., Wright, M. H., and Wright, P. E.: Convergence properties of the Nelder-Mead simplex method in low dimensions, SIAM J. of Optimiz., 9, 112–147, 1998.

Lipovetsky, S. and Conklin, M.: Analysis of regression in game theory approach, Appl. Stoch. Model. Bus., 17, 319–330, doi:10.1002/asmb.446, 2001.

Luhar, A. K. and Patil, R. S.: A general finite line source model for vehicular pollution prediction, Atmos. Environ., 23, 555–562, 1989.

Moller, P., Folkmann, J. K., Forchhammer, L., Brauner, E. V., Danielsen, P. H., Risom, L., and Loft, S.: Air pollution, oxidative damage to DNA, and carcinogenesis, Cancer Lett., 266, 84–97, doi:10.1016/j.canlet.2008.02.030, 2008.

Morawska, L., Jamriska, M., Thomas, S., Ferreira, L., Mengersen, K., Wraith, D., and McGregor, F.: Quantification of particle number emission factors for motor vehicles from on-road measurements, Environ. Sci. Technol., 39, 9130–9139, doi:10.1021/es050069c, 2005.

Morawska, L., Ristovski, Z., Jayaratne, E. R., Keogh, D. U., and Ling, X.: Ambient nano and ultrafine particles from motor vehicle emissions: Characteristics, ambient processing and implications on human exposure, Atmos. Environ., 42, 8113–8138, doi:10.1016/j.atmosenv.2008.07.050, 2008.

O'Brien, R. M.: A caution regarding rules of thumb for variance inflation factors, Qual. Quant., 41, 673–690, doi:10.1007/s11135-006-9018-6, 2007.

Pasquill, F.: The estimation of the dispersion of windborne material, Meteorol. Mag., 90, 33–49, 1961.

Pey, J., Querol, X., Alastuey, A., Rodriguez, S., Putaud, J. P., and Van Dingenen, R.: Source apportionment of urban fine and ultra-fine particle number concentration in a West-

ern Mediterranean city, Atmos. Environ., 43, 4407–4415, doi:10.1016/j.atmosenv.2009.05.024, 2009.

Polidori, A., Fine, P. M., Wilson, S., Koch, M., and Ayers, E.: Effect of proximity to a freeway with heavy-duty diesel traffic on the ambient concentrations of criteria and air toxic pollutants, 2009 National Ambient Air Monitoring Conference, Nashville, TN, 2009.

Quiros, D. C., Zhang, Q., Choi, W., He, M., Paulson, S. E., Winer, A. M., Wang, R., and Zhu, Y. F.: Near-roadways air quality impacts of a scheduled 36-hour closure of a major highway, Atmos. Environ., 67, 404–414, doi:10.1016/j.atmosenv.2012.10.020, 2013.

Seinfeld, J. H. and Pandis, S. N.: Atmospheric Chemistry and Physics: From Air Pollution to Climate Change, p. 918, John Willey & Sons, Inc., New York, NY, USA, 1998.

Sharma, P. and Khare, M.: Modelling of vehicular exhausts - a review, Transport. Res. D-Tr. E., 6, 179–198, doi:10.1016/s1361-9209(00)00022-5, 2001.

Sharan, M. and Yadav, A. K.: Simulation of diffusion experiments under light wind, stable conditions by a variable K-theory model, Atmos. Environ., 32, 3481–3492, doi:10.1016/s1352-2310(98)00048-x, 1998.

Stull, R. B.: An Introduction to Boundary Layer Meteorology, Kluwer Academic Publishers, Dordrecht, the Netherland, 1988.

Wang, Y. J. and Zhang, K. M.: Modeling near-road air quality using a computational fluid dynamics model, CFD-VIT-RIT, Environ. Sci. Technol., 43, 7778–7783, doi:10.1021/es9014844, 2009.

Westerdahl, D., Fruin, S., Sax, T., Fine, P. M., and Sioutas, C.: Mobile platform measurements of ultrafine particles and associated pollutant concentrations on freeways and residential streets in Los Angeles, Atmos. Environ., 39, 3597–3610, doi:10.1016/j.atmosenv.2005.02.034, 2005.

Zhang, K. M. and Wexler, A. S.: Evolution of particle number distribution near roadways – Part I: analysis of aerosol dynamics and its implications for engine emission measurement, Atmos. Environ., 38, 6643–6653, doi:10.1016/j.atmosenv.2004.06.043, 2004.

Zhang, K. M., Wexler, A. S., Zhu, Y. F., Hinds, W. C., and Sioutas, C.: Evolution of particle number distribution near roadways. Part II: the 'road-to-ambient' process, Atmos. Environ., 38, 6655–6665, doi:10.1016/j.atmosenv.2004.06.044, 2004.

Zhu, Y. F. and Hinds, W. C.: Predicting particle number concentrations near a highway based on vertical concentration profile, Atmos. Environ., 39, 1557–1566, 2005.

Zhu, Y. F., Kuhn, T., Mayo, P., and Hinds, W. C.: Comparison of daytime and nighttime concentration profiles and size distributions of ultrafine particles near a major highway, Environ. Sci. Technol., 40, 2531–2536, 2006.